Eur. Phys. J. A **13**, 155–161 (2002)

THE EUROPEAN PHYSICAL JOURNAL A

The case of RIB at intermediate energies: Isospin effects on nuclear dynamics

M. Di Toro[1,a], V. Baran[1,2], M. Colonna[1], V. Greco[1], S. Maccarone[1], and M. Cabibbo[1]

[1] Laboratori Nazionali del Sud and University of Catania, Via S. Sofia 44, I-95123 Catania, Italy
[2] NIPNE-HH, Bucharest, Romania

Received: 1 May 2001 / Revised version: 25 June 2001

Abstract. In the reaction dynamics of intermediate-energy radioactive beams we can probe highly asymmetric nuclear matter in compressed as well as dilute phases. In this report some predictions are presented, based on analytical results as well as on reaction simulations. We suggest a series of experiments with RIB aimed to shed light on isospin properties of nuclear interactions in the medium.

PACS. 21.65.+f Nuclear matter – 25.70.Pq Multifragment emission and correlations – 25.60.Pj Fusion reactions with unstable nuclei

1 Introduction

The starting point is that a key question in the physics of unstable nuclei is the knowledge of the EOS for asymmetric nuclear matter away from normal conditions. We note the effect of the symmetry term at low densities on the neutron skin structure, while the knowledge at high-densities region is crucial for supernovae dynamics and neutron star cooling. Effective interactions are obviously tuned to symmetry properties around normal conditions and any extrapolation can be quite dangerous. Microscopic approaches based on realistic NN interactions, Brueckner or variational schemes, or on effective field theories, show a quite large variety of predictions. In fig. 1 we collect the isospin dependence of some EOS which have *the same saturation properties for symmetric NM*: SkM* [1], SLy230b [2] and BPAL32 [3].

The aim of this paper is to discuss a series of reaction observables particularly sensitive to the symmetry term of the EOS.

In the following we shall refer to an "asy-stiff" EOS when we are considering a potential symmetry term linearly increasing with nuclear density and to an "asy-soft" EOS when the symmetry term shows saturation and eventually a decrease above normal density [4].

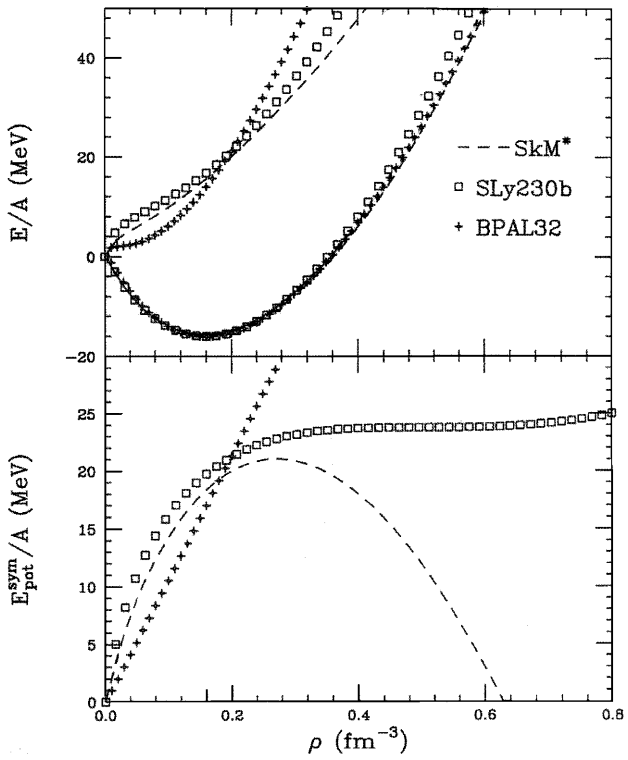

Fig. 1. EOS for various effective forces. Top: neutron matter (upper curves), symmetric matter (lower curves). Bottom: potential symmetry term.

2 Main mechanisms of dissipative collisions

We have studied isospin effects on the transition from fusion to deep inelastic and fragmentation. Particularly interesting is the neutron skin and neck dynamics. We follow the reaction dynamics using a new stochastic Boltzmann-Vlasov code [5]. In fig. 2 we show plots of the evolution of the density on the reaction plane for the mean trajectory

[a] e-mail: ditoro@lns.infn.it

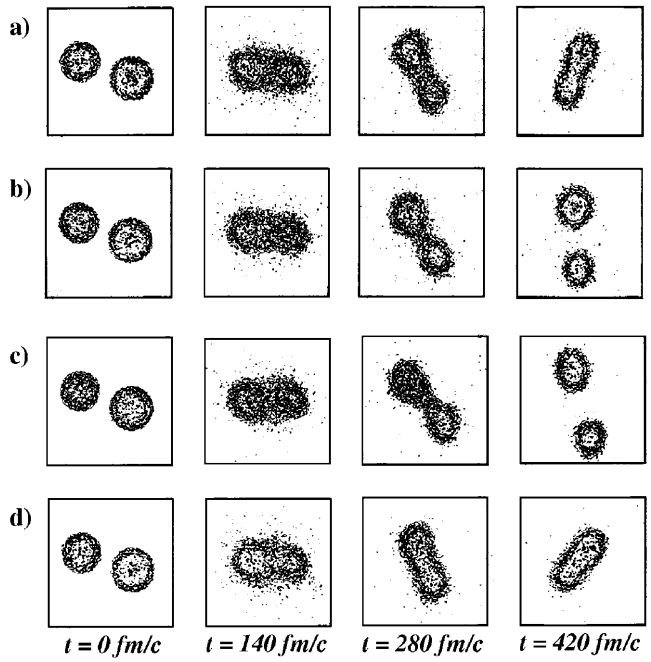

Fig. 2. Density plots: a) neutron-rich, asy-soft; b) neutron-rich, asy-stiff; c) proton-rich, asy-soft; d) proton-rich, asy-stiff.

(averaged over several events) for semicentral collisions ($b = 4$ fm) of neutron-rich (^{46}Ar+^{64}Ni) and neutron-poor (^{46}V + ^{64}Ge) ions at 30 A MeV.

The asy-soft choice leads to a less repulsive dynamics for neutron-rich colliding ions, which means a larger incomplete fusion cross-section at medium energies. For proton-rich systems we see just the opposite.

3 Multifragmentation

For charge asymmetric systems we expect a qualitative new feature in the liquid-gas phase transition, the onset of chemical instabilities that will show up in the novel nature of the unstable modes, given by a mixture of isoscalar and isovector components.

In the framework of Landau theory for two-component Fermi liquids, the spinodal border is determined by studying the stability of collective modes described by two coupled Landau-Vlasov equations for protons and neutrons.

In terms of the appropriate Landau parameters the stability condition can be expressed as [6]

$$(1 + F_0^{\rm nn})(1 + F_0^{\rm pp}) - F_0^{\rm np} F_0^{\rm pn} > 0\ . \qquad (1)$$

It is possible to show that this condition is equivalent to the following thermodynamical condition:

$$\left(\frac{\partial P}{\partial \rho}\right)_{T,y} \left(\frac{\partial \mu_{\rm p}}{\partial y}\right)_{T,P} > 0\,, \qquad (2)$$

discussed in [7,8], where $\mu_{\rm p}$ is the proton chemical potential and y the proton fraction. In fig. 3 we show the spinodal lines obtained from eq. (1) (continuous line with dots) which for asymmetric nuclear matter is seen to contain the lines corresponding to "mechanical instability", $\left(\frac{\partial P}{\partial \rho}\right)_{T,y} < 0$ (crosses). Therefore both eqs. (1),(2) describe the whole region of instability.

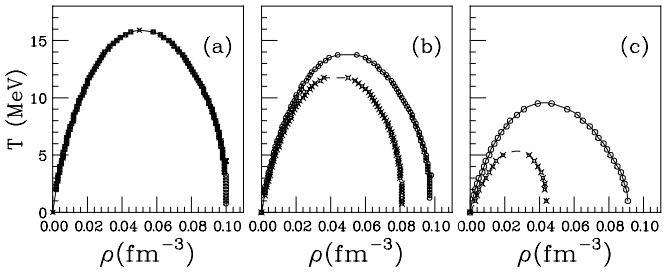

Fig. 3. Spinodal lines corresponding to chemical (joined points) and mechanical (crosses) instability for three asymmetries, $I = (N - Z)/(N + Z) = 0.0$,0.5,0.8 of nuclear matter.

We want to stress, however, that by just looking at the above stability conditions we cannot determine the nature of the fluctuations against which a binary system becomes chemically unstable. Indeed, the thermodynamical condition in eq. (2) cannot distinguish between two very different situations which can be encountered in nature: an attractive interaction between the two components of the mixture ($F_0^{\rm np}, F_0^{\rm pn} < 0$), as is the case of nuclear matter, or a repulsive interaction between the two species. We define density fluctuations as isoscalar-like when proton and neutron Fermi spheres (or equivalently the proton and neutron densities) fluctuate in phase and as isovector-like when the two Fermi spheres fluctuate out of phase. Then it is possible to prove, based on a thermodynamical approach of asymmetric Fermi-liquid mixtures [9], that chemical instabilities are triggered by isoscalar fluctuations in the first, *i.e.* attractive, situation and by isovector fluctuations in the second one. For the asymmetric nuclear-matter case, because of the attractive interaction between protons and neutrons, the phase transition is thus due to isoscalar fluctuations that induce chemical instabilities while the system is never unstable against isovector fluctuations. Of course the same attractive interaction is also at the origin of phase transitions in symmetric nuclear matter. However, in the asymmetric case isoscalar fluctuations lead to a more symmetric high-density phase everywhere under the instability line defined by eq. (1) [6, 9].

The Landau dispersion relation approach leads to a prediction of a very neutron-rich gas phase co-existing with an almost symmetric liquid phase formed in a dynamical non-equilibrium mechanism on short-time scales. Such "chemical effect" appears very sensitive to the symmetry term of the effective interaction used *below saturation density* [10].

Sensitive observables are the yield ratios of light isobars (*e.g.* t/^{3}He) and the formation of more stable primary intermediate mass fragments [11]. The space-time structure of the instabilities is discussed, with relative effects on fragment observables (mass/charge-correlations, kinetic energies, radial velocities) and on reaction

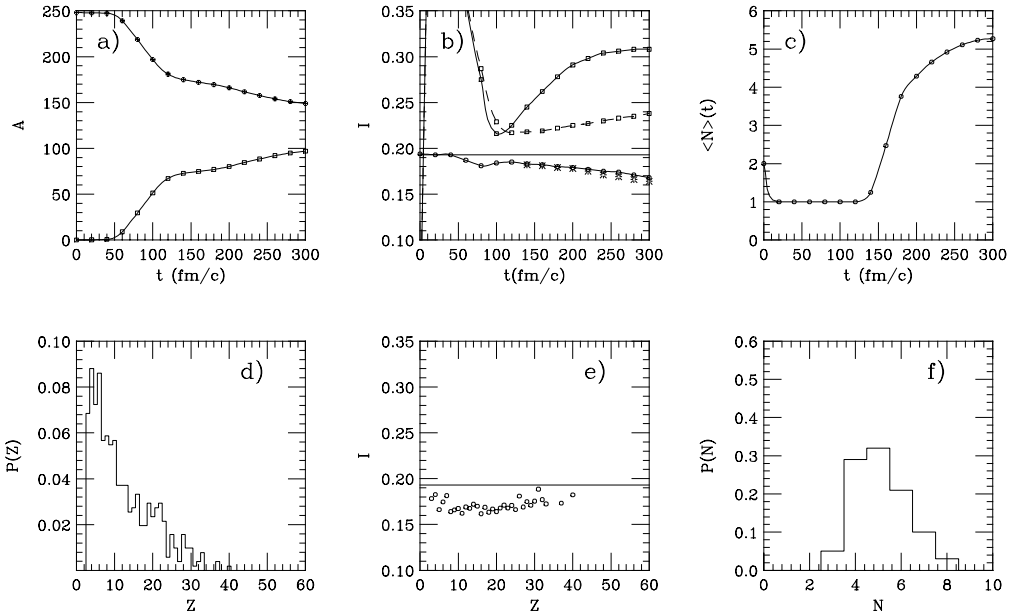

Fig. 4. ^{124}Sn + ^{124}Sn, 50 A MeV, $b = 2$ fm collisions: time evolution and freeze-out properties. See text. Asy-stiff EOS.

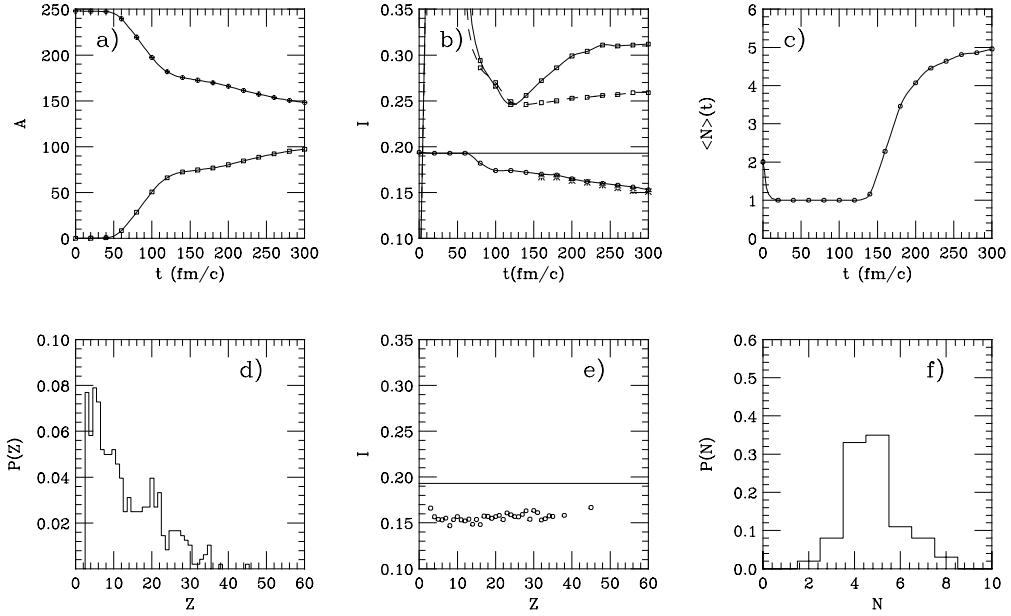

Fig. 5. As fig. 4: Asy-soft EOS.

mechanism scenarios (interaction times). Particularly important is the analysis of variances in connection to neck fragmentation events, which represent a large part of the reaction cross-section [12].

We have studied n-rich and n-poor Sn + Sn (124,112) collisions at 50 A MeV using a new stochastic transport approach with all isospin effects suitably accounted for [13]. For central collisions a chemical component in the spinodal instabilities is clearly seen. This effect is reduced in the neck fragmentation observed for semiperipheral collisions, pointing to a different nature of the instability. In spite of the low asymmetry tested with stable isotopes, the results are showing an interesting and promising dependence on the stiffness of the symmetry term, with an indication towards an increase of the repulsion above normal density.

A detailed analysis of the results from 200 events for the neutron-rich case is shown in figs. 4, 5 (central, $b =$ 2 fm) and figs. 6, 7 (peripheral, $b = 6$ fm). Each figure is organized in this way:

Top row, time evolution of: a) *Mass* in the liquid (upper curve) and gas (lower curve) phase; b) *Asymmetry* $I = (N - Z)/(N + Z)$ in the gas "central" (solid line and squares), gas total (dashed + squares), liquid "central" (solid + black dots) and clusters (stars). "Central" means in a cubic box of side 20 fm around the c.m. The

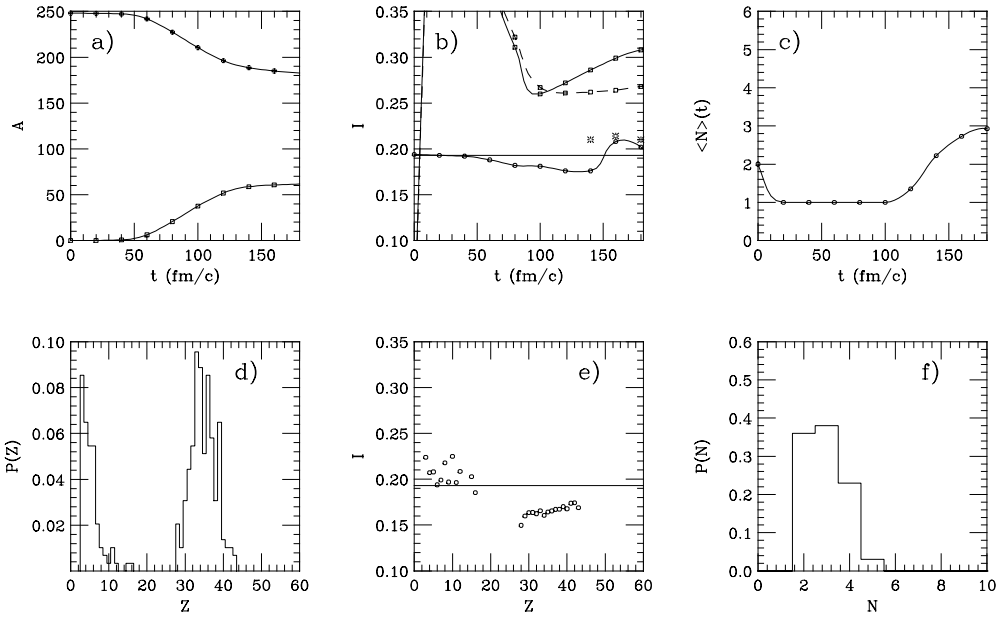

Fig. 6. ^{124}Sn + ^{124}Sn, 50 A MeV, $b = 6$ fm collisions: time evolution and freeze-out properties. See text. Asy-stiff EOS.

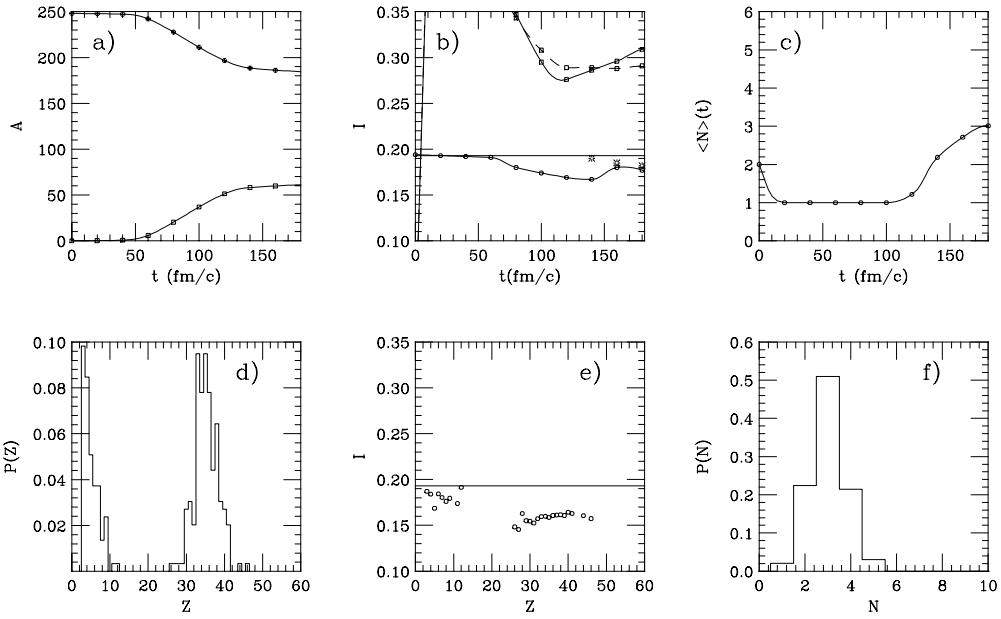

Fig. 7. As fig. 6: Asy-soft EOS.

horizontal line shows the initial average asymmetry; c) *Mean Fragment Multiplicity* $Z \geq 3$. The saturation of this curve defines the freeze-out configuration, as we can also check from the density plots.

Bottom row, properties of the "primary" fragments in the *Freeze-Out Configuration*: d) *Charge Distribution*, e) *Asymmetry Distribution* and f) *Fragment Multiplicity Distribution* (normalized to 1).

We see a neutron-dominated prompt particle emission and a second *neutron burst* at the time of fragment formation in the "central region". The latter is consistent with the dynamical spinodal mechanism in dilute asymmetric nuclear matter, as discussed before. The effect is quite reduced for semi-peripheral collisions (compare figs. 4b) and 6b)) and the IMFs ($3 \leq Z \leq 12$) produced in the neck are more neutron-rich (figs. 4e) and 6e)). This seems to indicate a different nature of the fragmentation mechanism in central and neck regions, *i.e.* a transition from volume to shape instabilities with different isospin dynamics. In more peripheral collisions the interaction time scale is also very reduced (fig. 6c) and this will quench the isospin migration.

In figs. 5, 7 we have the corresponding results for the *asy-soft* EOS. The main qualitative difference is a larger prompt neutron emission (compare the gas asymmetry in figs. 4b), 6b) with the corresponding figs. 5b), 7b)) joined

to a "slower" dynamics (see the c)-plots), as expected from the more attractive nature of the asymmetric EOS [4].

The interesting point is that the effect on fragment production is different for central and peripheral events. With respect to the *asy-stiff* case we have a smaller mean IMF multiplicity for central collisions (figs. 4f) *vs.* 5f)) and more fragments produced in the neck region (figs. 6f) *vs.* 7f)).

Neck instabilities have also the feature of forming clusters on the "spectator" side [12] leading to a "fission-like" splitting of the projectile-/target-like fragment. In our study of n-rich systems the rate of such dynamical fission processes is systematically larger for the asy-soft EOS, as expected from the previous discussion. This seems to be a quite sensitive observable to look at.

The most important qualitative difference of the neutron-poor case, ^{112}Sn + ^{112}Sn, is a larger prompt proton emission, in particular for central collisions. The number of protons available to produce clusters is then reduced with a related smaller mean IMF multiplicity. Moreover the reduction of the overall asymmetry is acting in the same direction.

Starting from the thermodynamical features of instabilities and the dynamics of phase transitions in binary systems we obtain a consistent description of the multifragmentation process in heavy-ion collisions and, in particular, of isospin effects. Isospin proves to be a useful probe in signaling a change in the fragment formation mechanism passing from central to semiperipheral collisions. Moreover this "isospin dynamics" is found to be quite sensitive to the symmetry term of the EOS, opening new stimulating perspectives on such studies, which are of great astrophysical interest, under laboratory controlled conditions.

4 Collective flows

The behaviour of the symmetry term above saturation density is strongly affecting the transverse flows measured in collisions of isobars with different charge asymmetries. The stiffness of the density dependence of the potential part of the symmetry energy is clearly linked to the balance energy for proton flows. Another sensitive observable seems to be the difference between neutron and proton flows for charge asymmetric systems, to be seen from measurements of the transverse flow of light isobars with different N/Z [14].

Also here the best overall results seem to be obtained with a "stiff" symmetry term, *i.e.* with a potential part of the symmetry energy per nucleon roughly linearly increasing with nuclear density up to about two times the saturation density, but again the asymmetry tested with stable beams is quite reduced. In fig. 8 we show the energy dependence of proton transverse flows for semicentral collisions of neutron-rich (^{58}Fe + ^{58}Fe) and neutron-poor (^{58}Ni + ^{58}Ni) evaluated in the asy-stiff case [14]. The balance energy shift and the overall agreement with the data of [15] is missing with the asy-soft choice.

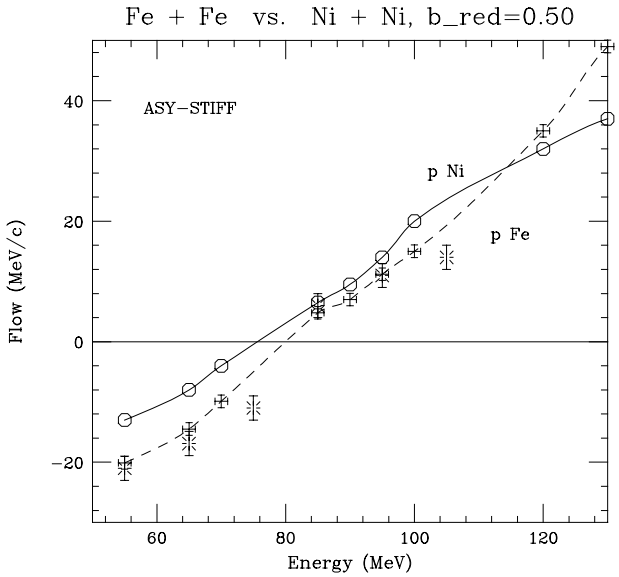

Fig. 8. Energy dependence of Fe-Fe *vs.* Ni-Ni proton transverse flows in semicentral collisions.

Particularly important would be to have good intensity beams to allow a "differential" study of the transverse flows, *i.e.* selecting different regions of transverse momentum of the emitted particles: this should allow a direct insight into the dynamical properties of the high-density region of the interacting asymmetric nuclear matter. Finally, it would be nice to study isospin effects on flows (transverse and elliptical) in the energy range 100–400 A MeV. In this energy region the momentum dependence of the mean field becomes extremely important. It seems then the right place to look at the role of isospin on effective masses for neutrons and protons, where quite amazingly divergent predictions are presently suggested [16–18].

The conclusion is that it would be very important to get some inputs coming from flow data for systems with different asymmetries in the region 100–400 A MeV, where we expect to have a larger contribution from the velocity-dependent part of the mean field and also where we should probe higher-density regions of matter still essentially made of neutrons and protons.

5 Pre-equilibrium effects

5.1 Gamma detection: the dynamical dipole

We only like to stress the interest in experiments on the pre-equilibrium. GDR gamma emission, ruled by the charge asymmetry in the entrance channel and by the fusion dynamics in the energy range 10–30 A MeV [19]. We can get important information on the isospin mixing dynamics and on the damping of the giant-dipole mode built on a hot and deformed dinuclear system and again on the symmetry term around saturation conditions.

To quantitatively show the effect, we present some results for the fusion reaction induced by ^{16}O ($N/Z = 1$) on ^{98}Mo ($N/Z = 1.33$). We have studied over a relative

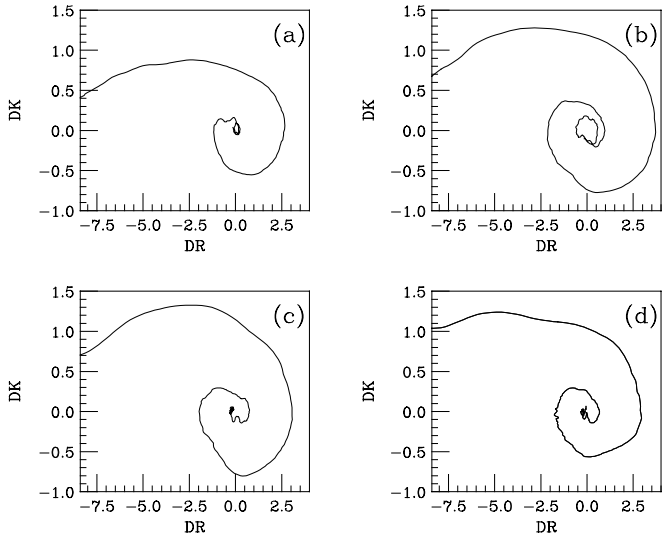

Fig. 9. Phase space trajectory of the entrance channel dipole for the O + Mo reaction: (a) to (d), beam energies 4 A MeV to 20 A MeV, see text.

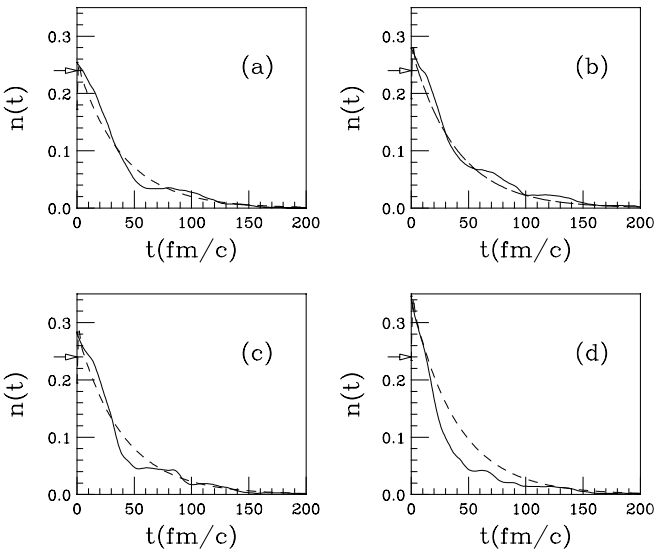

Fig. 10. Time evolution of the number of dipole phonons for the O + Mo reaction (solid lines). The dashed line is a reference curve with a constant spreading width (see text). The labels are as in fig. 9.

large range of incident energy, at 4, 8, 14, and 20 A MeV, the evolution of the composite system along the fusion path. We will consider central collisions, $b = 0$, as well representative of the features we are looking for.

At each time step we can evaluate the dinuclear dipole moment in coordinate and momentum space:

$$DR(t) \;=\; \frac{NZ}{A}X(t)\,; \quad DK(t) \;=\; \frac{\Pi(t)}{\hbar}\,. \qquad (3)$$

Here Π denotes the relative momentum $\Pi = \frac{NZ}{A}(\frac{P_{\rm p}}{Z} - \frac{P_{\rm n}}{N})$ with $P_{\rm p}$ ($P_{\rm n}$) the center-of-mass momentum for protons (neutrons), while $X = R_{\rm p} - R_{\rm n}$ is the distance between the centers of mass of the two components.

Figure 9 shows phase-space trajectories of the GDR, *i.e.* the time evolution of the DK-DR correlation. The spiral curves are nicely revealing an out-of-phase behaviour in the presence of some damping. The spiraling trend is starting at the touching configuration ($t = 0$, left points of the curves), a clear indication of a collective dipole response of the dinuclear system. The centre is reached when charge equilibration is achieved. From this time onwards the GDR mode will be only of statistical nature. The spiral shows a faster collapse to the central region at high beam energy (fig. 9(d)) since we have a larger damping of the dynamical collective motion.

We can also dynamically evaluate the time evolution of pre-equilibrium dipole phonons $n(t)$. We consider a harmonic oscillator description for the GDR:

$$H_{\rm GDR}(t) = \frac{\Pi^2(t)}{2M} + \frac{M\omega^2(t)}{2}X^2(t), \qquad (4)$$

where $M = \frac{ZN}{(Z+N)}m$ is the reduced mass of the neutron-proton relative motion, $m = 935\,$MeV being the nucleon mass.

At each time step the average number of phonons $n(t)$ can be determined from the simulations just dividing the total oscillator energy, as defined by eq. (4), by the one phonon energy at that instant, $\hbar\omega(t)$, *i.e.* corresponding to the deformation at the time t. The results are presented in fig. 10. The arrows show the initial value $n(0)$ predicted in a closed form without dynamical effects [19].

The dashed curve in all four pictures is the expected exponential decrease of the number of phonons using a constant spreading width value, $\Gamma^{\downarrow} = 5$ MeV. We note a quite good overall agreement at low beam energies 4 and 8 A MeV, (a) and (b). With increasing energy we clearly see in the number of phonons obtained from the simulations a faster damping which quickly compensates for the higher starting point. This is particularly evident at 20 A MeV (fig. 10(d)) where we have a considerably larger value for the spreading width, together with a sizeable kinetic term contribution to the initial number of phonons $n(0)$.

We see an interesting *rise and fall* of the effect with increasing beam energy, which is anyway well present in a relatively large range of energies, see fig. 9.

The dynamical nature of this dipole radiation will show up in a characteristic angular anisotropy, being related to a dipole oscillation in the reaction plane. Such a signal can then be eventually used to select fusion paths in RIB dissipative collisions.

5.2 Particle detection: N/Z content

We suggest the study of prompt neutron bursts for neutron-rich systems. We will get important information on the interplay between the compressibility of asymmetric NM, NN cross-sections and the symmetry term of the mean field. We note that the asy-stiff choice is more repulsive for neutrons at densities above ρ_0, where most of

the NN collisions will take place. Moreover in general the fast particle emission is strongly influenced by the momentum dependence of the mean field, in particular in the spectrum slopes and in the Fermi jet contributions [20, 21]. Such analysis for charge asymmetric collisions will bring direct information on isospin effects in the velocity-dependent part of the mean field, in regions above saturation density.

References

1. H. Krivine, J. Treiner, O. Bohigas, Nucl. Phys. A **336**, 155 (1980).
2. E. Chabanat, P. Bonche, P. Haensel, J. Meyer, R. Schaeffer, Nucl. Phys. A **627**, 710 (1997).
3. I. Bombaci, Phys. Rev. C **55**, 1 (1997). M. Prakash *et al.*, Phys. Rep. **280**, 1 (1997). We remark that a similar behaviour is obtained in the presently used relativistic mean-field approaches where the isovector contribution comes only from the ρ-meson and no exchange terms are taken into account. See the discussion in ref. [18].
4. M. Di Toro *et al.*, Progr. Part. Nucl. Phys. **42**, 125 (1999).
5. M. Colonna *et al.*, Phys. Rev. C **57**, 1410 (1998).
6. V. Baran *et al.*, Nucl. Phys. A **632**, 287 (1998).
7. L.D. Landau, E.M. Lifshitz, *Statistical Physics* (Pergamon Press, Oxford, 1980) p. 208
8. H.Mueller, B.D. Serot, Phys. Rev. C **52**, 2072 (1995).
9. V. Baran, M. Colonna, M. Di Toro, V. Greco, Phys. Rev. Lett. **86**, 4492 (2001).
10. M. Colonna, M. Di Toro, A.B. Larionov, Phys. Lett. B **428**, 1 (1998); M. Colonna *et al.*, in *Multifragmentation*, (GSI, Hirschegg, 1999) p. 322; V. Baran *et al.*, *What can we learn from nuclear instabilities?*, in *International Conference on Nuclear Physics, Bologna, 2000*, edited by G.C. Bonsignori *et al.*, Vol. **I** (World Scientific, 2001) pp. 293-298.
11. A.B. Larionov, A. Botvina, M. Colonna, M. Di Toro, Nucl. Phys. A **658**, 375 (1999).
12. M. Colonna, M. Di Toro, A. Guarnera, Nucl. Phys. A **589**, 160 (1995); J.D. Frankland, Thesis, Orsay, 1998; INDRA collaboration (B. Borderie), *International Winter Meeting on Nuclear Physics, Bormio* (RSEP, Università di Milano, 2000) p. 433.
13. M. Di Toro *et al.*, Nucl. Phys. A **681**, 426c (2001).
14. L. Scalone, M. Colonna, M. Di Toro, Phys. Lett. B **461**, 9 (1999).
15. G. Westfall, Nucl. Phys. A **630**, 27c (1998).
16. W. Zuo, I. Bombaci, U. Lombardo, Phys. Rev. C **60**, 024605 (1999) and references therein.
17. S. Kubis, M. Kutschera, Phys. Lett. B **399**, 191 (1997).
18. V. Greco *et al.*, *International Winter Meeting on Nuclear Physics, Bormio* (RSEP, Università di Milano, 2000) p. 314; Phys. Rev. C **63**, 035202 (2000); **64**, 045203 (2001).
19. V. Baran *et al.*, Nucl. Phys. A **600**, 111 (1996); M. Di Toro *et al.*, *The dynamical dipole mode*, in *International Conference on Giant Resonances, Osaka 2000*, Nucl. Phys. A **687**, 72 (2001); V. Baran *et al.*, Nucl. Phys. A **679**, 373 (2001).
20. P. Sapienza *et al.*, *International Winter Meeting on Nuclear Physics, Bormio* (RSEP, Università di Milano, 2000) p. 492; Phys. Rev. Lett. **87**, 2701 (2001).
21. V. Greco *et al.*, Phys. Rev. C **59**, 810 (1999).